Analytic dependence of the pressure and energy of an atomic fluid under shear

Gianluca Marcelli, B. D. Todd, and Richard J. Sadus
Centre for Molecular Simulation and School of Information Technology, Swinburne University of Technology, P.O. Box 218, Hawthorn, Victoria 3122, Australia
(Received 25 May 2000; published 24 January 2001)

Nonequilibrium molecular dynamics simulations are reported at different strain rates ($\dot{\gamma}$) for a shearing atomic fluid interacting via accurate two- and three-body potentials. We report that the hydrostatic pressure has a strain-rate dependence of $\dot{\gamma}^2$, in contrast to the $\dot{\gamma}^{3/2}$ dependence predicted by mode-coupling theory. Our results indicate that the pressure and energy of real fluids may display an analytic dependence on the strain rate. This is in contrast to previous work using either Lennard-Jones or Weeks-Chandler-Anderson potentials that had shown a $\dot{\gamma}^{3/2}$ dependence of pressure and energy.

DOI: 10.1103/PhysRevE.63.021204 PACS number(s): 61.20.Ja, 66.20.+d, 82.20.Wt, 83.50.Ax

I. INTRODUCTION

The transport properties of atomic and molecular fluids under shear are of significant scientific and technological interest. The dependence of the shear viscosity as a function of applied strain rate is of major importance in the design of suitable lubricants, and the viscoelastic properties of polymer melts under extensional and shear flows are important to the industrial processing of plastics. The structural design of molecules under appropriate flow fields can be aided by application of simulation methods such as nonequilibrium molecular dynamics (NEMD). In addition, NEMD can also be used to assess rheological models such as the Rouse or Doi-Edwards models of viscoelasticity for polymer solutions and melts [1], or the mode-coupling theory of Kawasaki and Gunton [2]. Of particular relevance for our current work is the mode-coupling theory, which predicts that in the limit of zero shear rate the shear viscosity is a nonanalytic function of the strain rate, $\eta \sim \dot{\gamma}^{1/2}$. This theory also predicts that the in-plane normal stress difference and the hydrostatic pressure both vary as $\dot{\gamma}^{3/2}$.

Typically, NEMD simulations are reported using either the Lennard-Jones or Weeks-Chandler-Anderson (WCA) intermolecular potentials to describe interatomic interactions (e.g., see references contained in [3,4]). However, both the Lennard-Jones and WCA potentials are effective multibody potentials and as such they do not represent two-body interactions accurately [5]. Earlier simulations [6,7] with these potentials appear to confirm the nonanalytic dependence of η on shear rate in the limit of low strain rate. However, more recent work questions the $\dot{\gamma}^{1/2}$ dependence of the shear viscosity. For example, Ryckaert *et al.* [8] found a $\dot{\gamma}^2$ dependence of the shear viscosity. The significance of these results is unclear because of the high strain rates and large statistical uncertainties in the data [9]. Furthermore, using profile biased thermostats under conditions of large strain rates can induce unwanted string phases in the fluid, which significantly reduce both the shear viscosity and the hydrostatic pressure from their true values [10,11]. Bhupathiraju, Cummings, and Cochran [12] demonstrate that in the limit of zero strain rate the shear viscosity behaves in a Newtonian manner, i.e., the shear viscosity becomes independent of $\dot{\gamma}$. Travis, Searles, and Evans [9] show that the shear viscosity may be fitted by a number of functions that do not have any theoretical basis. They also show that the viscosity profile may be successfully fitted by two separate linear functions of $\dot{\gamma}^{1/2}$ in two different strain-rate regimes. Alternatively, a Cross equation [13] and the Quentrec local-order theory for isotropic fluids [14–16] were also found to give reasonable agreement with simulation data.

Mode-coupling theory does not provide guidance on how small the strain rate must be in order to observe the predicted $\dot{\gamma}^{1/2}$ and $\dot{\gamma}^{3/2}$ dependence for the shear viscosity and hydrostatic pressure, respectively. As NEMD simulations are typically performed at relatively high rates of strain to obtain high signal to noise ratios, such simulations cannot confirm the predictions of mode-coupling theory. In the absence of simulation data at field strengths several orders of magnitude smaller than those typically achievable, the question of the validity of mode-coupling theory remains open. However, most previous NEMD simulations using effective multibody intermolecular potentials have shown that the hydrostatic pressure and internal energy *do* behave as predicted by the theory, even at these relatively high strain rates.

We are aware of only one previous NEMD study of simple atomic fluids interacting via accurate two- and three-body intermolecular potentials. Lee and Cummings [17,18] reported NEMD simulations of planar Couette flow for a system of 108 atoms interacting via a potential composed of the Barker-Fisher-Watts (BFW) two-body potential [5] plus the three-body triple-dipole potential of Axilrod and Teller (AT) [19]. The three-body interaction was observed to reduce the value of the shear viscosity by only 3%. In the range of strain rates studied, Lee and Cummings found that the strain-rate behavior of the energy, pressure, and shear viscosity all conformed to the predictions of mode-coupling theory.

In this work, we report NEMD simulations of the shear viscosity of argon interacting via the Barker-Fisher-Watts [5] and Axilrod-Teller [19] intermolecular potentials. An adequate system size of 500 atoms was used resulting in greater statistical accuracy than reported elsewhere [17,18]. We show that the pressure is clearly not a linear function of $\dot{\gamma}^{3/2}$, but can be well described by an analytic $\dot{\gamma}^2$ dependence. This relationship is independent of the three-body potential interaction and is only a consequence of two-body interactions.

Our results also demonstrate that the shear viscosity is not necessarily a linear function in $\dot{\gamma}^{1/2}$. The statistical accuracy of the viscosity data is not sufficient, however, to unambiguously determine an accurate dependence on the strain rate.

II. SIMULATION DETAILS

A. Intermolecular potentials

The total intermolecular potential (ϕ) is a contribution from two-body interactions ($\phi^{(2)}$) and three-body dispersion interactions ($\phi^{3\,\mathrm{BDisp}}$):

$$\phi(r)=\phi^{(2)}(r)+\phi^{3\,\mathrm{BDisp}}(r). \tag{1}$$

Several accurate two-body potentials are available in the literature [20] and a recent review is available [21]. The two-body interaction of argon is well represented by the Barker-Fisher-Watts potential [5]. The BFW potential is a linear combination of the Barker-Pompe [22] (ϕ_{BP}) and Bobetic-Barker [23] (ϕ_{BB}) potentials

$$\phi^{(2)}(r)=0.75\phi_{\mathrm{BB}}(r)+0.25\phi_{\mathrm{BP}}(r), \tag{2}$$

where the potentials of Barker-Pompe and Bobetic-Barker have the form

$$\phi(r)=\epsilon\left[\sum_{i=0}^{5}A_i(x-1)^i\exp[\alpha(1-x)]-\sum_{j=0}^{2}\frac{C_{2j+6}}{\delta+x^{2j+6}}\right] \tag{3}$$

In Eq. (3), $x=r/r_m$ where r_m is the intermolecular separation at which the potential has a minimum value, and the other parameters are obtained by fitting the potential to experimental data for molecular beam scattering, second virial coefficients, and long-range interaction coefficients. The contribution from repulsion has an exponential dependence on intermolecular separation, and the contribution to dispersion of the C_6, C_8, and C_{10} coefficients is included. The only difference between the Barker-Pompe and Bobetic-Barker potentials is that a different set of parameters is used in each case. These parameters were taken from the literature [5].

There are many possible contributions to three-body dispersion interactions [21,24] involving contributions from such factors as third-order triple-dipole, dipole-dipole-quadrupole, dipole-quadrupole-quadrupole, quadrupole-quadrupole-quadrupole, and fourth-order triple-dipole interactions. However, recent work [25,26] has clearly established that there is a large degree of cancellation between the contributions and that the triple-dipole interaction alone is an accurate representation of three-body dispersion interactions. The triple-dipole potential was evaluated from the formula proposed by Axilrod and Teller [19]:

$$\phi_{DDD}(ijk)=\frac{\nu_{DDD}(1+3\cos\theta_i\cos\theta_j\cos\theta_k)}{(r_{ij}r_{ik}r_{jk})^3}, \tag{4}$$

where ν_{DDD} is the nonadditive coefficient, and the angles and intermolecular separations refer to a triangular configuration of atoms. The nonadditive coefficient for argon (518.3 a.u.) was taken form the literature [27]. Recent work [25,28–32] indicates that the Axilrod-Teller term can significantly improve the prediction of liquid phase properties.

B. NEMD Algorithm

The NEMD simulations were performed by applying the standard SLLOD equations of motion for planar shear flow [3]. The SLLOD equations for a one-component atomic fluid flowing with streaming velocity u_x in the x direction and constant strain rate $\dot{\gamma}=\partial u_x/\partial y$ are

$$\dot{\mathbf{r}}_i=\frac{\mathbf{p}_i}{m}+\mathbf{i}\dot{\gamma}y_i, \tag{5a}$$

$$\dot{\mathbf{p}}_i=\mathbf{F}_i-\mathbf{i}\dot{\gamma}p_{yi}-\alpha\mathbf{p}_i, \tag{5b}$$

where $\mathbf{r}_i$ is the laboratory position of atom i, $\mathbf{p}_i$ is the peculiar (i.e., thermal) momentum of atom i, m is the atomic mass (set to a reduced value of 1 in our simulations), and $\mathbf{F}_i$ is the total intermolecular force (including two and three-body contributions) on atom i. α is a Gaussian thermostat multiplier used to keep the kinetic temperature of the fluid constant:

$$\alpha=\frac{\sum_{i=1}^{N}[\mathbf{F}_i\cdot\mathbf{p}_i-\dot{\gamma}p_{xi}p_{yi}]}{\sum_{i=1}^{N}\mathbf{p}_i\cdot\mathbf{p}_i}. \tag{6}$$

The equations of motion are integrated by a fouth-order Gear predictor-corrector scheme [33], with a reduced integration time step ($t^*=t\sqrt{\epsilon/m\sigma^2}$) of 0.001. A nonequilibrium simulation trajectory is typically run for 250 000 time steps. Averages are taken over five independent trajectories, each starting at a new configuration. To equilibrate the system, each trajectory is first run without a shearing field. After the shearing field is switched on, the first 50 000 time steps of each trajectory are ignored, and the fluid is allowed to relax to a nonequilibrium steady state. Thus, every pressure, energy and viscosity data point represents a total run length of $5\times200\,000=10^6$ time steps.

The two-body potentials were truncated at half the box length and appropriate long-range correction terms were evaluated to recover the contribution to the pressure and energy for the full intermolecular potential [5]. Some care needs to be taken with the three-body potentials because the application of a periodic boundary can potentially destroy the spatial invariance of three particles [34,25]. In earlier work [25] the behavior of the three-body terms for many thousands of different orientations and intermolecular separations was examined. All the three-body terms asymptote rapidly to zero with increasing intermolecular separation. For a system size of 500 or more atoms, at the liquid density studied, truncating the three-body potentials at intermolecular separations of a quarter of the length of the simulation box was observed to be an excellent approximation to the full potential. This also avoided the problem of three-body invariance to periodic boundary conditions.

The long-range corrections for the three-body energies and pressures were calculated as

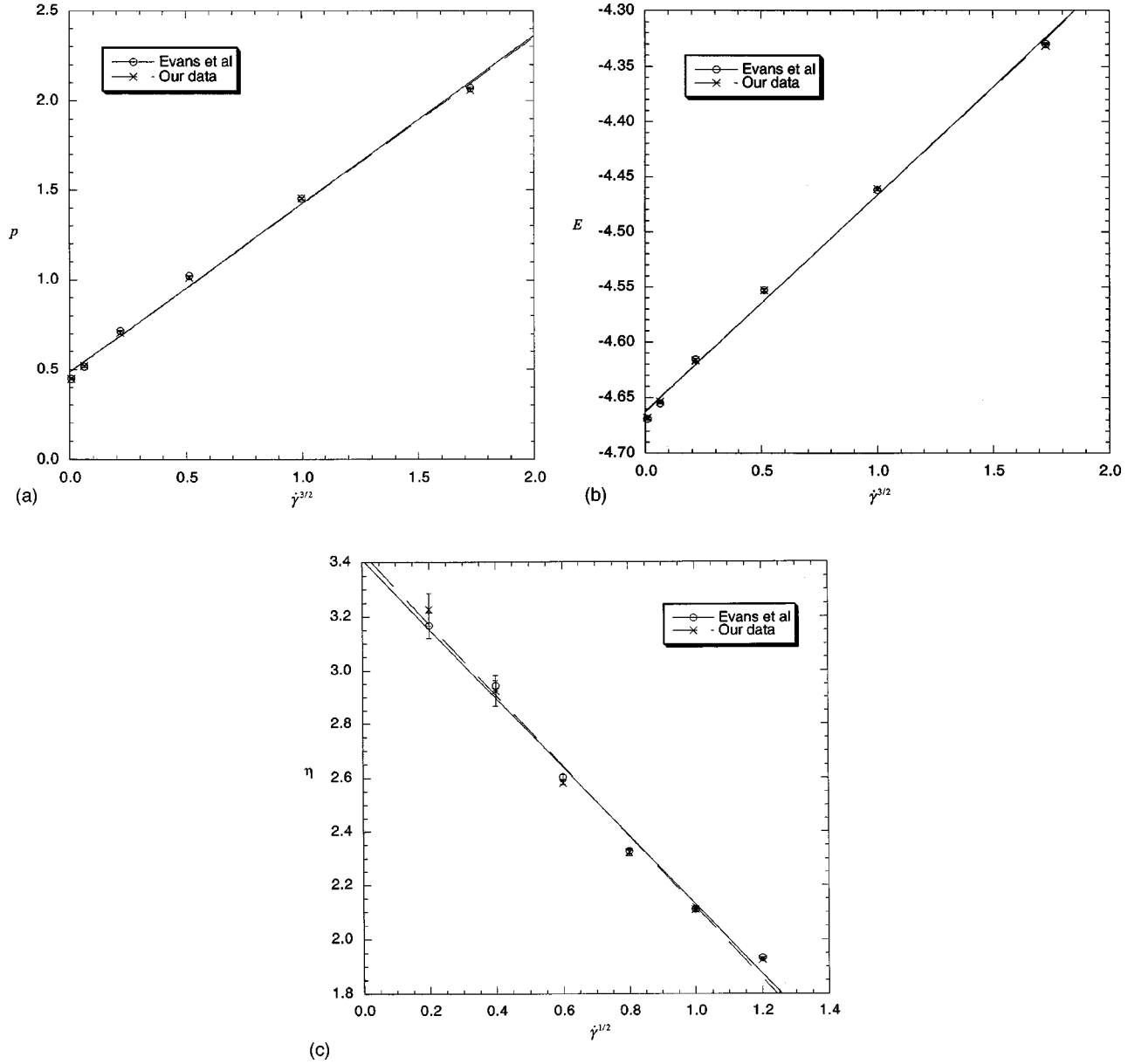

FIG. 1. (a) Comparison of pressure data of Evans, Morriss, and Hood [35] with our own for a system of 2048 Lennard-Jones atoms. The pressure displays the expected $\dot{\gamma}^{3/2}$ dependency. (b) The same, but for energy. (c) Viscosity profile.

$$E^{(3)}_{\text{long range}} = N\rho^2 \int_{r_{12}<r_{13}<r_{23}} \int_{R^{(2)}_{\text{cutoff}}<r_{23}} g^{(3)}(r_{12},r_{13},r_{23}) \times \phi_{DDD}(r_{12},r_{13},r_{23}) d\mathbf{r}_{12} d\mathbf{r}_{13}, \tag{7a}$$

$$p^{(3)}_{\text{long range}} = \frac{3E^{(3)}_{\text{long range}}}{V}, \tag{7b}$$

where we use the superposition approximation of Barker, Fisher, and Watts [5]:

$$g^{(3)}(r_{12},r_{13},r_{23}) = g^{(2)}(r_{12}) g^{(2)}(r_{13}) g^{(2)}(r_{23}) \tag{7c}$$

with $g^{(2)}(r_{23})$ set to unity.

Before applying the SLLOD algorithm to the BFW fluid, we repeated simulations on a Lennard-Jones fluid, reported by Evans, Morriss, and Hood [35] for a system of 2048 atoms with a cutoff radius of 3.5σ. Our simulations were in excellent agreement with these results, and are displayed in Fig. 1. The pressures and energies were found to vary linearly with $\dot{\gamma}^{3/2}$, whereas the viscosity varied as $\dot{\gamma}^{1/2}$, as previously observed. We further note that all subsequent simulations performed on the BFW fluid are made with exactly the same computer program. The only difference is the form of the intermolecular potentials, and hence forces, used in the calculation of fluid properties. This limits any possible errors that could be introduced by comparing results generated from different code.

III. RESULTS AND DISCUSSION

The results of NEMD simulations for the pressure, energy, and shear viscosity of argon at different strain rates are

TABLE I. Pressure, energy, and viscosity data for the BFW potential, with and without the three body AT potential. Standard errors are represented by a single digit enclosed in parentheses, and imply that the error is in the last decimal place. Two and three-body long-range corrections are included.

	BFW potential			BFW+AT potentials		
$\dot{\gamma}$	p	E	η	p	E	η
0.0	−0.103(2)	−3.682(2)		0.017(2)	−3.557(1)	
0.078	−0.105(1)	−3.683(1)	0.72(2)	0.019(2)	−3.555(1)	0.72(3)
0.1755	−0.108(1)	−3.679(1)	0.754(5)	0.020(2)	−3.554(1)	0.742(6)
0.24	−0.102(2)	−3.683(2)	0.747(6)	0.022(1)	−3.552(1)	0.732(6)
0.312	−0.103(2)	−3.677(1)	0.753(2)	0.024(2)	−3.551(1)	0.733(5)
0.4	−0.099(1)	−3.673(1)	0.747(1)	0.031(2)	−3.550(1)	0.725(1)
0.5	−0.092(4)	−3.667(3)	0.746(6)	0.034(3)	−3.541(1)	0.725(6)
0.702	−0.079(2)	−3.656(1)	0.727(2)	0.054(1)	−3.529(1)	0.719(1)
0.9555	−0.050(1)	−3.631(2)	0.715(1)	0.084(2)	−3.511(1)	0.703(2)
1.248	0.002(1)	−3.595(1)	0.699(1)	0.135(1)	−3.480(1)	0.689(1)
1.5795	0.076(1)	−3.558(1)	0.677(1)	0.214(1)	−3.443(1)	0.668(1)
1.95	0.179(2)	−3.506(1)	0.653(1)	0.312(2)	−3.396(1)	0.644(1)

reported in Table I. The normal convention was adopted for the reduced density ($\rho^*=\rho\sigma^3$), temperature ($T^*=kT/\varepsilon$), energy ($E^*=E/\varepsilon$), pressure ($p^*=p\sigma^3/\varepsilon$), viscosity [$\eta^*=\eta\sigma^2(m\varepsilon)^{-1/2}$], and strain rate ($\dot{\gamma}^*=\dot{\gamma}[\sigma(m/\varepsilon)^{1/2}]$). Unless otherwise stated, all quantities quoted in this work are in terms of these reduced quantities and the superscript * will be omitted. All simulations were performed at the state point $(\rho,T)=(0.592\ [1.034\,\mathrm{g\,cm^{-3}}],\ 0.95\ [135\ \mathrm{K}])$. This point was chosen because it is representative of the liquid phase of argon, being approximately midway between the triple point and the critical point. The number of atoms in our systems was $N=500$, and the size of our simulation cell, L, was 9.453 reduced units. The three-body terms were truncated at $0.25L$, whereas the two-body terms were truncated at $0.5L$. These cutoff distances further ensured that the total nonequilibrium pair distribution function was constant (i.e., equal to unity) over the range of r where long-range corrections are applied. Potential parameters were taken from the literature [5].

The uncertainties in the time averages for the energy, pressure, and viscosity reported in Table I represent the standard errors of the averages over the five independent nonequilibrium trajectories. The data include calculations with the BFW potential alone and a combined BFW+AT potential. We confirmed that the two- and three-body energies and pressures at equilibrium were correct by comparing them with independent calculations of these quantities obtained by the Gibbs ensemble method [36]. These results, and various attempts to fit the simulation data, are illustrated in Figs. 2–4.

Mode-coupling theory predicts that the pressure of a fluid under shear has a linear dependence with $\dot{\gamma}^{3/2}$. To test this prediction, we plot the total pressure of the fluid against $\dot{\gamma}^{3/2}$ in Fig. 2(a). If the pressure were a linear function of $\dot{\gamma}^{3/2}$ one would expect random statistical fluctuations in the data points about the linear fit. However, a careful analysis of the data suggests a systematic deviation from the expected $\dot{\gamma}^{3/2}$ linear behavior.

In Fig. 2(b) the total pressure is presented as a function of $\dot{\gamma}^2$. We find that the pressure is more closely represented by an analytic $\dot{\gamma}^2$ dependence. In Table II the coefficients of the two fits are presented, as well as their respective errors. Additionally, the coefficients of both fitted equations and the absolute average deviations (AADs) [37] are given. The AAD is a measure of the overall accuracy of the agreement between the fits and the simulation data. This analysis clearly indicates that a $\dot{\gamma}^2$ relationship describes the dependence of the pressure with strain rate more accurately than fitting the data using $\dot{\gamma}^{3/2}$. Recent work [48] using a truncated and shifted Lennard-Jones potential also suggests a possible $\dot{\gamma}^2$ dependence away from the triple point.

At equilibrium, a pressure of approximately 1 MPa is predicted compared with an experimental value of 4 MPa [38]. The main contribution to the overall pressure comes from the kinetic component and two-body interactions, which are of similar magnitude but of opposite sign. This means that small statistical fluctuations in the two-body contribution can greatly affect both the magnitude and sign of the total pressure.

To determine whether the $\dot{\gamma}^2$ dependence is due to the addition of three-body interactions, we plot the two-body and full two- plus three-body contributions to the total pressure separately in Fig. 2(b). The results for the two-body pressures are obtained from simulations involving only the two-body BFW potential interactions, without the three-body terms. It is evident that the $\dot{\gamma}^2$ dependence is caused by two-body interactions. The three-body contributions serve only to shift the pressures higher by approximately 0.1 reduced units. Although it could be reasonably expected that the three-body contribution to the total pressure may depend on strain rate, our simulation results suggest that any dependence is very weak for the strain rates covered.

The configurational energy per particle is presented as a function of $\dot{\gamma}^{3/2}$ and $\dot{\gamma}^2$ in Figs. 3(a) and 3(b). The E vs $\dot{\gamma}^{3/2}$ plot does show a systematic departure from linearity, though the departure is not as pronounced as that observed for the

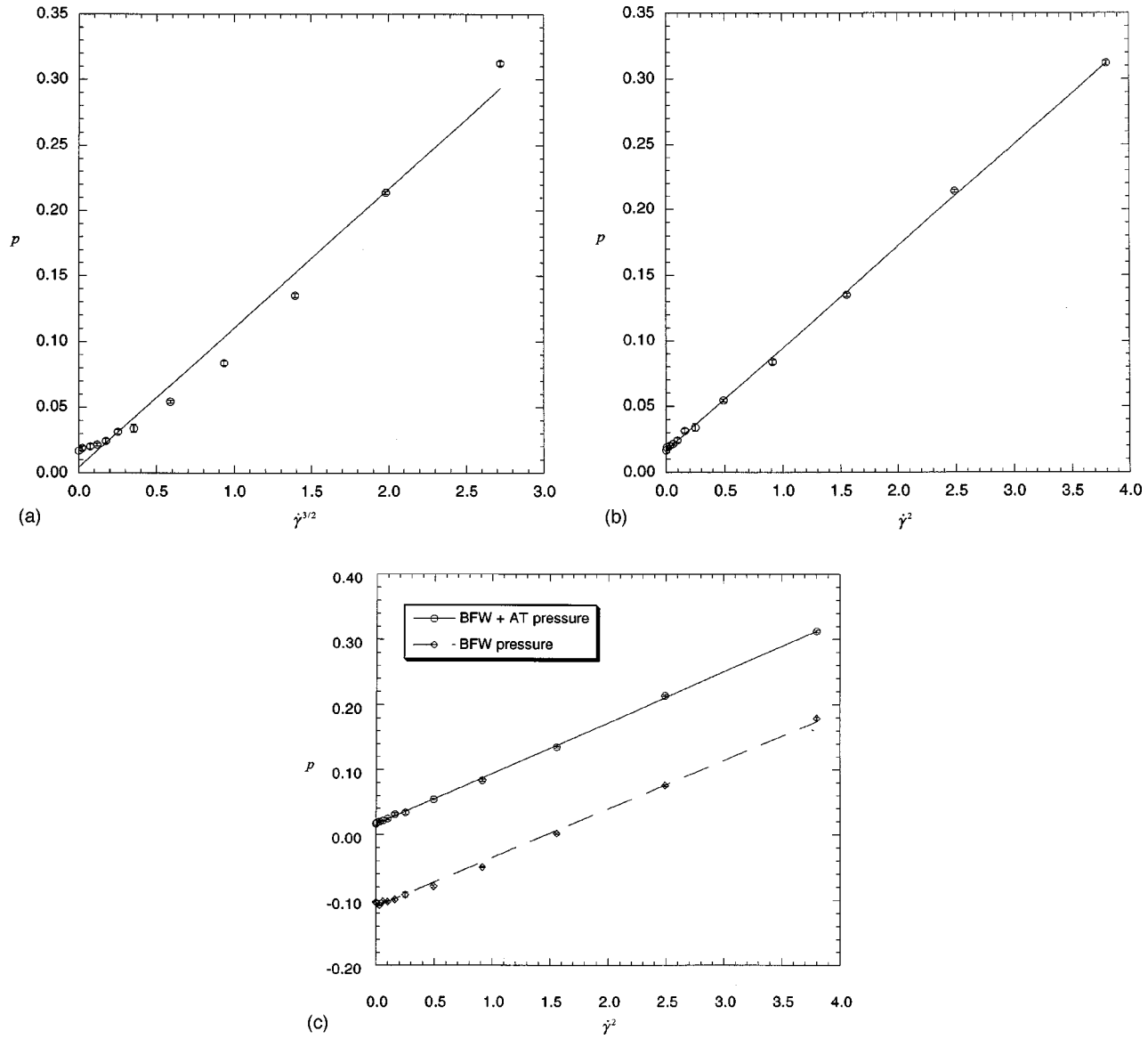

FIG. 2. Total two- plus three-body pressure as a function of (a) $\dot{\gamma}^{3/2}$ and (b) $\dot{\gamma}^2$. (c) Potential contributions to the two- and two-body+three-body pressures as functions of $\dot{\gamma}^2$.

pressure. The coefficients of the fit along with the absolute average deviation are also presented in Table II. It is clear that based on these data alone either a $\dot{\gamma}^{3/2}$ or a $\dot{\gamma}^2$ dependence is an equally viable representation of the strain-rate variation of the energy.

The shear viscosity of the fluid, calculated as $\eta=-(P_{xy}+P_{yx})/2\dot{\gamma}$, is plotted against $\dot{\gamma}$ in Fig. 4. The viscosity is not a simple function of $\dot{\gamma}^{1/2}$, which is consistent with the conclusion reached by Travis, Searles, and Evans [9]. The statistical errors in our viscosity measurements are not sufficiently small to unambiguously determine the functional form of the viscosity profile. Any fit of η vs $\dot{\gamma}^n$ is reasonable, where $\frac{1}{2}\leqslant n\leqslant 2$. However, when the data are extrapolated to zero strain rate, the values of the equilibrium viscosity predicted by the $\dot{\gamma}$, $\dot{\gamma}^{3/2}$, and $\dot{\gamma}^2$ fits $[(757\pm1)\times10^7$, $(741\pm1)\times10^7$, and $(733\pm1)\times10^7\,\mathrm{N\,s\,m^{-2}}$, respectively] are in good agreement with the experimental value of $740.2\times10^7\,\mathrm{N\,s\,m^{-2}}$ [38]. The $\dot{\gamma}^{1/2}$ fit actually gives the worst agreement $[(805\pm3)\times10^7\,\mathrm{N\,s\,m^{-2}}]$ with experiment.

In-plane and out-of-plane viscosities were also calculated from our simulations. However, the statistical accuracy of the results was not sufficiently good to form any conclusions as to their functional dependence on the strain rate. Therefore, these results are not recorded here.

Our results differ from those of Lee and Cummings [17,18], who observed the standard $\dot{\gamma}^{3/2}$ dependence of the pressure with strain rate. Lee and Cummings used a system size of 108 atoms for both the BFW and BFW+AT calculations. Quantitative error estimates were not reported with their data. Normally, large errors in pressure can be expected for simulations involving such a small number of atoms, which can hinder the correct identification of the strain-rate dependency of pressure. We repeated their simulations for 108 particles at the same state point, and present the results

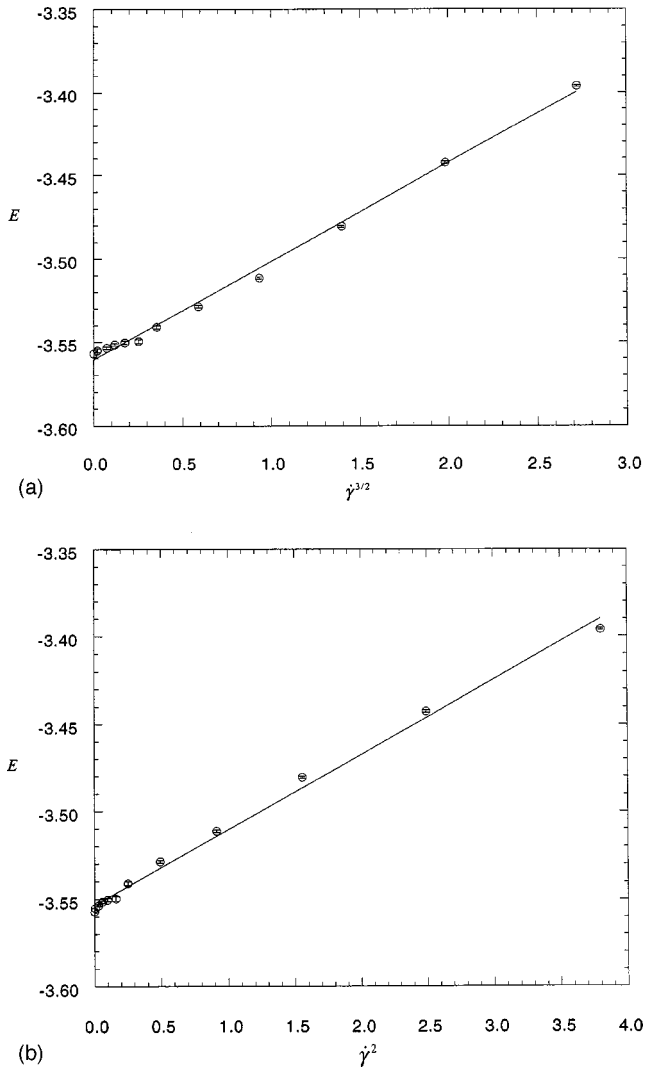

FIG. 3. Configurational energy of the fluid as a function of (a) $\dot{\gamma}^{3/2}$ and (b) $\dot{\gamma}^2$.

for the total two- plus three-body pressure and energy dependence on strain rate in Figs. 5 and 6, respectively. Our simulations were performed by time averaging over a total of 2×10^6 time steps, and our statistics are thus more reliable. We do not include long-range corrections in this set of data, which would only add a constant term to shift the pressure and energy profiles. It does not change the shape, which is what we are interested in. Once again our results confirm the $\dot{\gamma}^2$ dependence of both pressure and energy.

We make the observation that a system size of 108 particles is actually too small to account fully for all the possible three-body interactions. The cutoff value for the three-body potential should not exceed one-quarter of the length of the simulation cell, for geometrical constraints imposed by the three-body interactions [25]. In their system, Lee and Cummings used a cell length L of 5.67 reduced units. Their cutoff radius was $0.5L=2.835$, which is too large for their small system size. It is primarily for such reasons that we chose to study a larger system size of 500 atoms.

The pressure tensor of the fluid was calculated by the

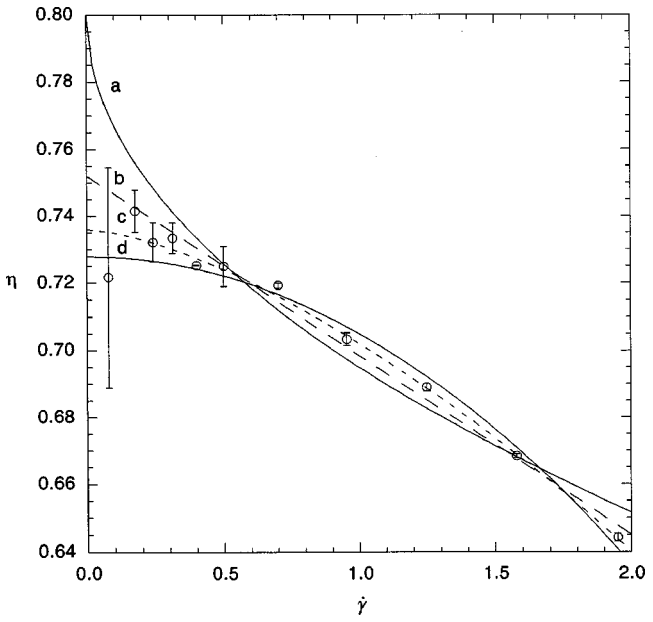

FIG. 4. Shear viscosity as a function of $\dot{\gamma}$. The lines illustrate different fits with strain-rate dependency to the power of (a) 0.5, (b) 1, (c) 1.5, and (d) 2.

standard Irving-Kirkwood expression [39], modified to include three-body contributions:

$$\langle \mathsf{P} \rangle = \frac{1}{V}\left\langle \sum_{i=1}^{N} m_i[\mathbf{v}_i-\mathbf{u}(\mathbf{r}_i)][\mathbf{v}_i-\mathbf{u}(\mathbf{r}_i)] + \sum_{i=1}^{N-1}\sum_{j>i}^{N} \mathbf{r}_{ij}\mathbf{F}_{ij}^{(2)} + \sum_{i=1}^{N-2}\sum_{j>i}^{N-1}\sum_{k>j}^{N} [\mathbf{r}_{ij}\mathbf{F}_{(ij)k}^{(3)} + \mathbf{r}_{ik}\mathbf{F}_{(ik)j}^{(3)} + \mathbf{r}_{jk}\mathbf{F}_{(jk)i}^{(3)}] \right\rangle; \tag{8}$$

where $\mathbf{F}_{(\alpha\beta)\gamma}^{(3)} = -\partial\phi_{\alpha\beta\gamma}/\partial\mathbf{r}_{\alpha\beta}\cdot\mathbf{u}(\mathbf{r}_i)$ is the streaming velocity of the fluid at $\mathbf{r}_i$, $\mathbf{v}_i$ is the velocity of atom i measured in the laboratory frame, and we note that for the SLLOD algorithm $\mathbf{p}_i \equiv \mathbf{v}_i - \mathbf{u}(\mathbf{r}_i)$. $\mathbf{F}_{ij}^{(2)}$ is the two-body interaction force, and terms involving $\mathbf{F}_{(\alpha\beta)\gamma}^{(3)}$ are the corresponding three-body

TABLE II. Coefficients of the various fits to the total (two- plus three-body) pressure, energy, and viscosity profiles of Figs. 2–4. Also included are the absolute average deviations as percentages.

	a	b	AAD (%)
$p=a+b\dot{\gamma}^{3/2}$	0.0032(6)	0.1039(5)	26.72
$p=a+b\dot{\gamma}^{2}$	0.0164(6)	0.0781(4)	3.97
$E=a+b\dot{\gamma}^{3/2}$	−3.5607(4)	0.0592(3)	0.08
$E=a+b\dot{\gamma}^{2}$	−3.5554(4)	0.0430(2)	0.09
$\eta=a+b\dot{\gamma}^{1/2}$	0.800(2)	−0.105(2)	1.60
$\eta=a+b\dot{\gamma}$	0.752(1)	−0.0535(8)	0.74
$\eta=a+b\dot{\gamma}^{3/2}$	0.7360(8)	−0.0339(5)	0.45
$\eta=a+b\dot{\gamma}^{2}$	0.7279(7)	−0.0229(3)	0.69

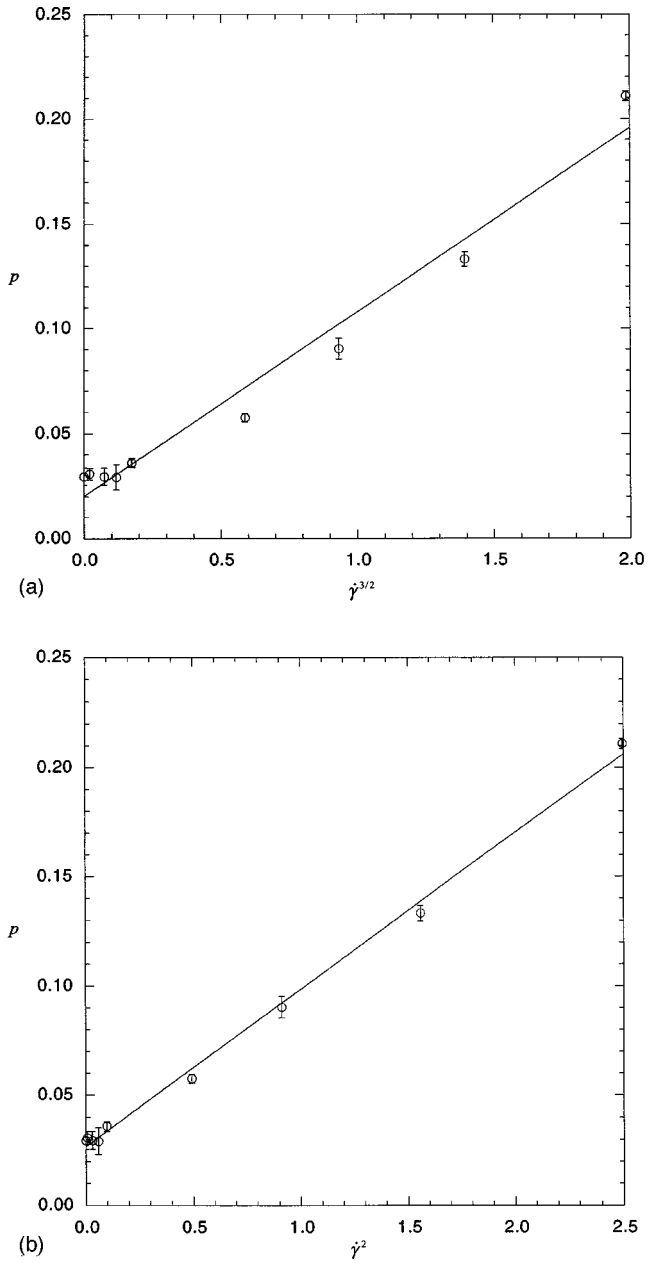

FIG. 5. Total two-plus three-body pressure as a function of (a) $\dot{\gamma}^{3/2}$ for a system of 108 atoms, AAD=17.89, and (b) $\dot{\gamma}^2$, AAD =6.09.

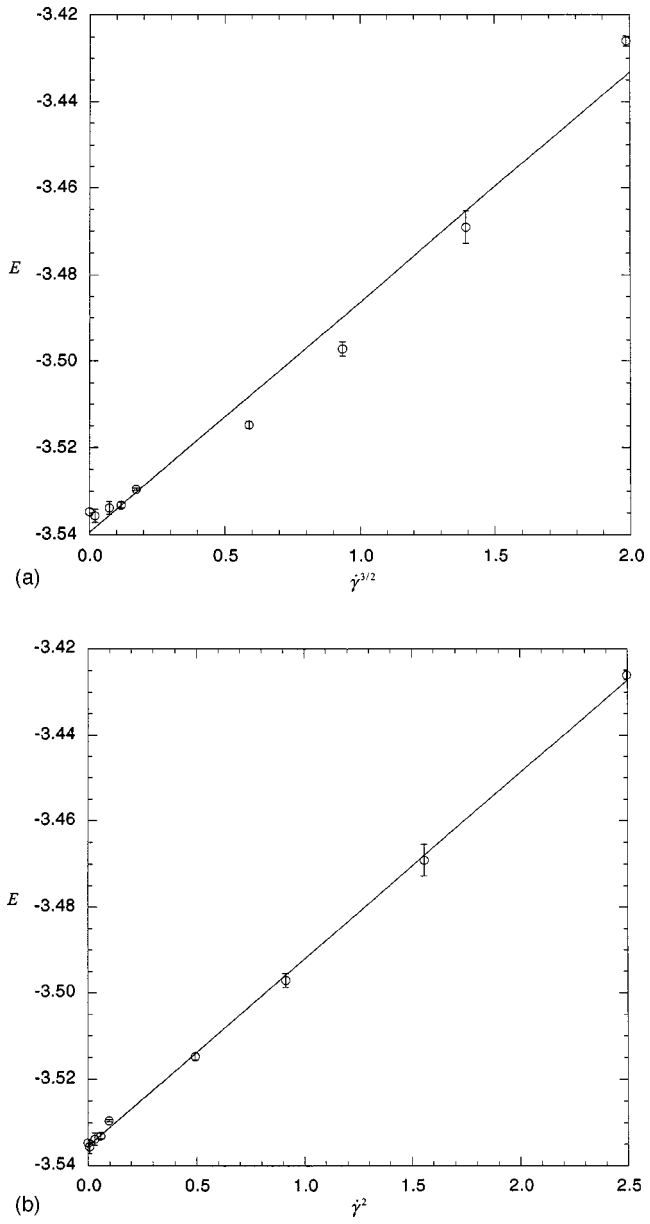

FIG. 6. Configurational energy of the 108-atom system as a function of (a) $\dot{\gamma}^{3/2}$ and (b) $\dot{\gamma}^2$. AADs are 0.11 and 0.04, respectively.

contributions to the total force. As previously pointed out, the calculation of the pressure tensor involved not only time averaging of the steady-state pressure, but also averaging over a number of independent simulations, each starting at different equilibrium atomic configurations.

To check that there was no error in the evaluation of Eq. (8), we calculated the pressure tensor by another independent method, namely, by integrating over the *total* nonequilibrium pair distribution function. This method will allow us to calculate the two-body contribution to the pressure. The three-body contribution to the pressure was checked by the relationship $p^{(3)}=3E^{(3)}/V$ [5,40].

We can expand the nonequilibrium pair distribution function as a Taylor series, and consider only terms that are first order in the gradient of the streaming velocity [41], i.e.,

$$g^n(\mathbf{r},\nabla\mathbf{u}(\mathbf{r}))=g(r,\nabla\mathbf{u}(\mathbf{r}))+\nu(r,\nabla\mathbf{u}(\mathbf{r}))\left(\frac{\mathbf{rr}}{r^2}\right):\nabla\mathbf{u}(\mathbf{r}) + (\nu_0(r,\nabla\mathbf{u}(\mathbf{r}))-\tfrac{1}{3}\nu(r,\nabla\mathbf{u}(\mathbf{r})))\nabla\cdot\mathbf{u}(\mathbf{r}), \tag{9}$$

where $g(r,\nabla\mathbf{u}(\mathbf{r}))$ is the usual pair distribution function and $\nu(r,\nabla\mathbf{u}(\mathbf{r}))$ represents the radial part of the distortion from spherical symmetry of the nonequilibrium pair distribution function. For constant volume deformation, $\nabla\cdot\mathbf{u}(\mathbf{r})=0$ and so Eq. (9) simplifies to

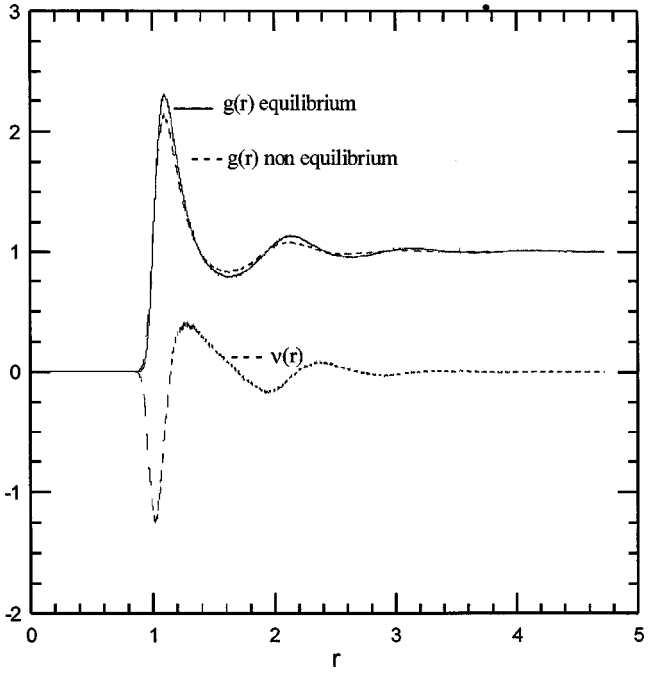

FIG. 7. $g(r)$ and $\nu(r)$ for the fluid shearing at the highest strain rate of $\dot{\gamma}=1.95$.

$$g^n(\mathbf{r},\nabla\mathbf{u}(\mathbf{r}))=g(r,\nabla\mathbf{u}(\mathbf{r}))+\nu(r,\nabla\mathbf{u}(\mathbf{r}))\left\langle\frac{\mathbf{rr}}{r^2}\right\rangle:\nabla\mathbf{u}(\mathbf{r}). \tag{10}$$

Following the procedure outlined by Pryde [42–44], one can show that $\nu(r,\nabla\mathbf{u}(\mathbf{r}))$ for a three-dimensional fluid shearing in the *x*-*y* plane is

$$\nu(r,\dot{\gamma})=15\left\langle\frac{x_{ij}y_{ij}}{r_{ij}^2}\right\rangle\Big/\ 8\pi\dot{\gamma}\rho r^2 dr, \tag{11}$$

where ρ is the fluid density, $x_{ij}=x_i-x_j$, $y_{ij}=y_i-y_j$, $r_{ij}=r_i-r_j$, and the averaging is performed in a small region of the fluid between r and $r+dr$. The two-body configurational component of the pressure may be calculated from the virial as

$$p_\phi^{(2)}=(2/3)\pi\rho^2\int_0^\infty g(r,\dot{\gamma})r^3\frac{\partial\phi^{(2)}(r)}{\partial r}dr. \tag{12}$$

Note that $\nu(r,\dot{\gamma})$ contributes only to the off-diagonal elements of the pressure tensor and so does not appear in Eq. (12). However, it will appear in the shear stress, and hence shear viscosity. The two-body contributions to the shear viscosity and total internal energy are, respectively, determined as

$$\eta_\phi^{(2)}=(2\pi/15)\rho^2\int_0^\infty\nu(r,\dot{\gamma})r^3\frac{\partial\phi^{(2)}(r)}{\partial r}dr \tag{13}$$

and

$$E_\phi^{(2)}=2\pi N\rho\int_0^\infty g(r,\dot{\gamma})r^2\phi^{(2)}dr. \tag{14}$$

We display $g(r,\dot{\gamma})$ and $\nu(r,\dot{\gamma})$ for the fluid shearing with a strain rate of $\dot{\gamma}=1.95$ in Fig. 7. Additionally, we include $g(r,\dot{\gamma}=0)$ at equilibrium for comparison purposes. The difference between $g(r,\dot{\gamma})$ for $\dot{\gamma}=0$ and 1.95 reflects the change in the fluid structure with imposed strain rate, which is to be expected. It is well known that $g(\mathbf{r},\dot{\gamma})$ is no longer spherically symmetric at large values of $\dot{\gamma}$ [3], but becomes distorted at an angle of 45° to the fluid velocity streamlines.

In Table III we show the two-body components of the pressure, energy, and viscosity calculated by Eqs. (12)–(14) alongside the direct values for a number of values of $\dot{\gamma}$. For every value of $\dot{\gamma}$, the quantities were calculated over a single trajectory of 50 000 time steps. Very good agreement (up to the fourth decimal place) is found between the direct calculations and those involving $g(r,\dot{\gamma})$ and $\nu(r,\dot{\gamma})$. This agreement suggests that the observed dependencies of the pressure, energy, and viscosity on strain rate are not a result of an error in the direct calculations of these properties.

There is an additional check we can perform to ensure that the SLLOD algorithm was correctly implemented, and that the pressures and shear stresses were correctly calculated. For a thermostated fluid, the energy dissipation may be expressed as

$$\dot{H}(t)=-V\mathsf{P}:\nabla\mathbf{u}-\alpha\sum_{i=1}^{N}\frac{\mathbf{p}_i\cdot\mathbf{p}_i}{m}. \tag{15}$$

For a shearing fluid Eq. (15) reduces to

$$\dot{H}(t)=-VP_{xy}\dot{\gamma}-\alpha\sum_{i=1}^{N}\frac{\mathbf{p}_i\cdot\mathbf{p}_i}{m}, \tag{16}$$

TABLE III. Two-body components of pressure, energy, and viscosity calculated by the direct method and via $g(r,\dot{\gamma})$ and $\nu(r,\dot{\gamma})$ [see Eqs. (12)–(14)]. Errors are not quoted, nor are long-range corrections included.

	$p_{2\text{-body}}$		$E_{2\text{-body}}$		$\eta_{2\text{-body}}$	
$\dot{\gamma}$	(simulation)	$[g(r,\dot{\gamma})]$	(simulation)	$[g(r,\dot{\gamma})]$	(simulation)	$[\nu(r,\dot{\gamma})]$
0.0	−0.7136	−0.7136	−3.6384	−3.6382		
0.702	−0.6720	−0.6720	−3.6118	−3.6118	0.6017	0.6016
0.9555	−0.6382	−0.6383	−3.5941	−3.5941	0.5899	0.5899
1.248	−0.5869	−0.5870	−3.5547	−3.5547	0.5837	0.5837
1.549	−0.5018	−0.5019	−3.5165	−3.5165	0.5671	0.5671
1.95	−0.4045	−0.4046	−3.4738	−3.4738	0.5436	0.5436

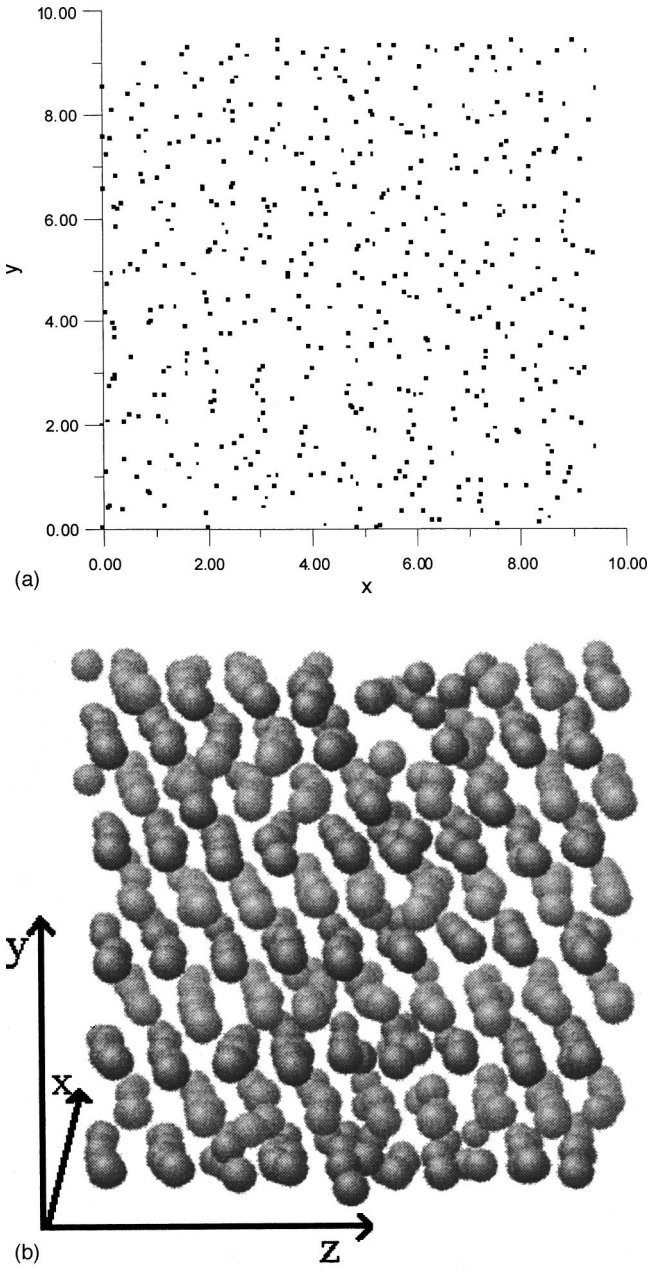

FIG. 8. (a) Two-dimensional projection onto the *x*-*y* plane of a three-dimensional snapshot of the fluid shearing at the highest strain rate of $\dot{\gamma}=1.95$. There is no evidence of string formation. (b) Full three-dimensional snapshot of the fluid shearing at a high value of $\dot{\gamma}=11$. Strings are now clearly discernible.

where $\dot{H}(t)$ is the time derivative of the total internal energy. For (a) the algorithm to be working correctly and (b) the shear stress to be correctly calculated, the right-hand side (RHS) of Eq. (16) must equal the left-hand side for all *t*. This was indeed found to be the case in all our simulations, but for brevity we do not include the data in this paper. Additionally, we checked that the hydrostatic pressure calculation was correct by calculating the dissipation for a fluid undergoing planar elongation. The dissipation is related to differences in the diagonal elements of the pressure tensor, and so Eq. (15) reduces to [45]

$$\dot{H}(t)=-V\dot{\varepsilon}[P_{xx}-P_{yy}]-\alpha\sum_{i=1}^{N}\frac{\mathbf{p}_i\cdot\mathbf{p}_i}{m}. \tag{17}$$

Here $\dot{\varepsilon}$ is the elongation strain rate, and the fluid expands in the *x* direction while simultaneously contracting in the *y* direction. Details of the simulation algorithm for planar elongation can be found elsewhere [45,46]. Our simulations confirmed the equivalence of the RHS and LHS of Eq. (17).

Previous work [8] that had attempted to show the analytic dependence of the viscosity on $\dot{\gamma}^2$ was criticized for the relatively high rates of strain used [9]. Large strain rates can induce unwanted string phases, i.e., highly ordered solidlike configurations. These string phases arise for high Reynolds number flows, where the assumption of a linear streaming velocity profile is questionable. The linear profile is imposed upon the flow via the SLLOD equations of motion. For a freely shearing system with Lee-Edwards periodic boundary conditions, high Reynolds number flows should exhibit an S-shaped kink in the streaming velocity profile. If the assumed (linear) and actual streaming velocities are not the same, the thermostat interprets this deviation as heat, and applies an additional force to the equation of motion for the momenta [see Eq. (5b)]. It is this additional force appearing in the term involving α that serves to stabilize the linear velocity profile and enhance the ordering of the fluid by reducing the rate of entropy production. Once the fluid's ordering is enhanced, its viscosity and pressure are reduced dramatically from their true values, which can lead to incorrect dependencies on $\dot{\gamma}$.

In Fig. 8(a) we project a three-dimensional snapshot of the fluid onto a two-dimensional surface in the *x*-*y* plane. The fluid was sheared at the highest value of $\dot{\gamma}$ that we simulated, $\dot{\gamma}=1.95$. There is no obvious enhancement in the structure of the fluid. For our system, strings were only noticeable at very high values of $\dot{\gamma}$, typically $\dot{\gamma}>5$. This is in contrast to work by Evans *et al.* [11], who found evidence of strings for values of $\dot{\gamma}$ as low as ~ 2. However, their simulations were performed on a Weeks-Chandler-Anderson fluid [47]. Our simulations have been performed on BFW fluids, both with and without the additional three-body term, where the range over which fluid atoms interact is significantly greater than for WCA fluids. In Fig. 8(b) we show a full three-dimensional snapshot of the fluid sheared at $\dot{\gamma}=11$, where now the appearance of strings is very pronounced. If strings were formed in our simulations, the anticipated side effect should be to dramatically reduce the values of the viscosity and hydrostatic pressure at higher strain rates. Our data clearly do not support this.

Finally, we checked the dependence of the pressure, energy, and viscosity profiles on the size of the cutoff potential radius used. While the results presented here were performed with a two-body cutoff radius of $r_c^{(2)}=0.5L=4.726$, we also performed simulations at a smaller cutoff of $r_c^{(2)}=2.28$ for a system of 500 atoms. The shapes of these profiles remained unchanged.

IV. CONCLUSIONS

We have demonstrated that use of accurate two- and three-body potentials for shearing liquid argon displays significant departure from the expected strain-rate dependencies of the pressure, energy, and shear viscosity. The pressure is convincingly observed to vary linearly with an apparent analytic $\dot{\gamma}^2$ dependence, in contrast to the predicted $\dot{\gamma}^{3/2}$ dependence of mode-coupling theory. This dependence results primarily from the two-body potential. The three-body term serves only to raise the magnitude of the total pressure. The dependence of the energy on strain rate could also vary as $\dot{\gamma}^2$, but a $\dot{\gamma}^{3/2}$ dependence is also possible, and we are unable to unambiguously distinguish between them. Further work is required to resolve this issue. The shear viscosity is also seen not to be a simple function of $\dot{\gamma}^{1/2}$, and our data are in general agreement with recent work of other authors. Our best extrapolation of the zero-shear viscosity gives excellent agreement (within 1%) with the known experimental value of $740.2\times10^{7}\ \mathrm{N\,s\,m^{-2}}$.

ACKNOWLEDGMENTS

G.M. thanks the Australian government for financial support. Generous allocations of computer time on the Fujitsu VPP300 and NEC SX-4/32 computers were provided by the Australian National University Supercomputer Centre and the CSIRO High Performance Computing and Communications Centre, respectively. We also wish to thank J. Ge for assistance with some simulations.

[1] M. Doi and S. F. Edwards, *The Theory of Polymer Dynamics* (Clarendon, Oxford, 1986).
[2] K. Kawasaki and J. D. Gunton, Phys. Rev. A **8**, 2048 (1973).
[3] D. J. Evans and G. P. Morriss, *Statistical Mechanics of Nonequilibrium Liquids* (Academic, London, 1990).
[4] S. S. Sarman, D. J. Evans, and P. T. Cummings, Phys. Rep. **305**, 1 (1998).
[5] J. A. Barker, R. A. Fisher, and R. O. Watts, Mol. Phys. **21**, 657 (1971).
[6] D. J. Evans, Phys. Rev. A **22**, 290 (1980).
[7] D. J. Evans, Phys. Rev. A **23**, 1988 (1981).
[8] J.-P. Ryckaert, A. Bellemans, G. Ciccotti, and G. V. Paolini, Phys. Rev. Lett. **60**, 128 (1988).
[9] K. P. Travis, D. J. Searles, and D. J. Evans, Mol. Phys. **95**, 195 (1998).
[10] D. J. Evans and G. P. Morriss, Phys. Rev. Lett. **56**, 2172 (1986).
[11] D. J. Evans, S. T. Cui, H. J. M. Hanley, and G. C. Straty, Phys. Rev. A **46**, 6731 (1992).
[12] R. Bhupathiraju, P. T. Cummings, and H. D. Cochran, Mol. Phys. **88**, 1665 (1996).
[13] M. M. Cross, J. Colloid Sci. **20**, 417 (1965).
[14] B. Quentrec, J. Mec. **20**, 449 (1981).
[15] B. Quentrec, Mol. Phys. **46**, 707 (1982).
[16] C. Trozzi and G. Ciccotti, Phys. Rev. A **29**, 916 (1984).
[17] S. H. Lee and P. T. Cummings, J. Chem. Phys. **99**, 3919 (1993).
[18] S. H. Lee and P. T. Cummings, J. Chem. Phys. **101**, 6206 (1994).
[19] B. M. Axilrod and E. Teller, J. Chem. Phys. **11**, 299 (1943).
[20] G. C. Maitland, M. Rigby, E. B. Smith, and W. A. Wakeham, *Intermolecular Forces, Their Origin and Determination* (Clarendon, Oxford, 1981).
[21] R. J. Sadus, *Molecular Simulation of Fluids: Theory, Algorithms and Object-Orientation* (Elsevier, Amsterdam, 1999).
[22] J. A. Barker and A. Pompe, Aust. J. Chem. **21**, 1683 (1968).
[23] M. V. Bobetic and J. A. Barker, Phys. Rev. B **2**, 4169 (1970).
[24] M. A. van der Hoef and P. A. Madden, J. Chem. Phys. **111**, 1520 (1999).
[25] G. Marcelli and R. J. Sadus, J. Chem. Phys. **111**, 1533 (1999).
[26] G. Marcelli and R. J. Sadus, J. Chem. Phys. **112**, 6382 (2000).
[27] P. J. Leonard and J. A. Barker, in *Theoretical Chemistry: Advances and Perspectives*, Vol. 1, edited by H. Eyring and D. Henderson (Academic, London, 1975).
[28] G. Marcelli and R. J. Sadus, High Temp.-High Press. (to be published).
[29] R. J. Sadus and J. M. Prausnitz, J. Chem. Phys. **104**, 4784 (1996).
[30] R. J. Sadus, Fluid Phase Equilibria **150-151**, 63 (1998).
[31] R. J. Sadus, Ind. Eng. Chem. Res. **37**, 2977 (1998).
[32] R. J. Sadus, Fluid Phase Equilibria **144**, 351 (1998).
[33] C. W. Gear, *Numerical Initial Value Problems in Ordinary Differential Equations* (Prentice-Hall, Englewood Cliffs, NJ, 1971).
[34] P. Attard, Phys. Rev. A **45**, 5649 (1992).
[35] D. J. Evans, G. P. Morriss, and L. M. Hood, Mol. Phys. **68**, 637 (1989).
[36] A. Z. Panagiotopoulos, N. Quirke, M. Stapleton, and D. J. Tildesley, Mol. Phys. **63**, 527 (1988).
[37] R. J. Sadus, J. Phys. Chem. **99**, 12 363 (1995).
[38] N. B. Vargaftik, *Handbook of Physical Properties of Liquids and Gases* (Hemisphere, Washington, DC, 1975).
[39] J. H. Irving and J. G. Kirkwood, J. Chem. Phys. **18**, 817 (1950).
[40] E. Rittger, Comput. Phys. Commun. **67**, 412 (1992).
[41] H. S. Green, *The Molecular Theory of Fluids* (North-Holland Interscience, New York, 1952).
[42] J. A. Pryde, *The Liquid State* (Hutchinson University Library, London, 1966).
[43] W. T. Ashurst and W. G. Hoover, Phys. Rev. A **11**, 658 (1975).
[44] H. J. M. Hanley and D. J. Evans, Mol. Phys. **39**, 1039 (1980).
[45] B. D. Todd, Phys. Rev. E **56**, 6723 (1997).
[46] B. D. Todd and P. J. Daivis, Comput. Phys. Commun. **117**, 191 (1999).
[47] J. D. Weeks, D. Chandler, and H. C. Andersen, J. Chem. Phys. **54**, 5237 (1971).
[48] M. Matin, P. J. Daivis and B. D. Todd, J. Chem. Phys. **113**, 9122 (2000).